Journal of Himalayan Earth Sciences Volume, No., 2026 pp. 1-19

Mineralogical Characteristics and Adsorption Potential of Reservoir-Derived Rock Samples from Eastern Saudi Arabia: Implications for Environmental Remediation

Ruaa Mohammed Almotawa[1*]

[1]*Department of Chemistry, College of Science, University of Hafr Al Batin, Hafr Al Batin, 31991, Saudi Arabia*

**Email: ralmotawa@uhb.edu.sa , ORCID: https://orcid.org/0000-0002-6181-7001*

Submitted Date: 15/12/2025 Acceptance Date: 10/07/2026 Publication Date:---------

Abstract

This study investigates subsurface reservoir-derived rock samples collected during oil well drilling operations at depths of 2000 ft and 4000 ft in an oil reservoir in eastern Saudi Arabia, aiming to evaluate their mineralogical characteristics and adsorption potential. The samples were characterized using X-ray diffraction (XRD), Fourier-transform infrared spectroscopy (FTIR), scanning electron microscopy (SEM), energy-dispersive X-ray spectroscopy (EDS), Brunauer–Emmett–Teller (BET) surface area measurements, thermogravimetric analysis (TGA), and ultraviolet–visible spectroscopy (UV–Vis). The 2000-ft sample has a silicate-dominated composition, with XRD and FTIR identifying quartz, feldspar, and clay-related components. In contrast, the 4000-ft sample is carbonate-dominated, with calcite as the major mineral phase. SEM observations revealed differences in grain arrangement and the visibility of intergranular spaces between the two depth intervals, consistent with the observed mineralogical variations. BET analysis showed a moderate specific surface area of 23.225 m^2/g for the 2000-ft sample, suggesting measurable potential for adsorption applications. UV–Vis measurements indicated hydrocarbon-associated absorption features, with relatively stronger signals observed in the shallower sample. Thermogravimetric analysis further revealed distinct thermal behaviors between the two samples. The results demonstrate that mineralogical composition and depth-related variation significantly influence the structural and adsorption potential characteristics of reservoir-derived materials. The silicate-dominated 2000-ft sample exhibits more favorable adsorption potential than the deeper carbonate-dominated sample, highlighting the importance of mineralogical variability in evaluating the environmental application potential of subsurface reservoir materials.

***Keywords*:** Reservoir rocks, Oil reservoir, Adsorption, Mineralogical analysis, Environmental remediation, XRD, Surface area.

1. Introduction

Recently, growing interest in biomass and raw materials has been driven by their unique physicochemical properties and wide availability (Chakraborty et al., 2022). Sandstone has gained attention due to its extensive applications, including building materials, thermal energy reservoir mediums, water filtration materials, and manufacturing bricks and ceramics. It is defined as a loose granular material formed from the weathering and disintegration of rocks and other geological formations, ranging in diameter from 0.0625 to 2 mm (Kumar et al., 2018; Bell, 1992; Cao et al., 2022; Noruzi et al., 2024; Kumar et al., 2017). Sandstone is one of the two main forms, along with carbonate, usually present in crude oil reservoirs (Worden et al., 2018). Generally, sandstone can be found in deserts, land, and river environments, whereas carbonate rocks can exist in the marine environment due to

the abundance of aquatic organisms and calcium deposits (Arsalan et al., 2013). The geological processes, including compaction and cementation, form sandstones containing compressed quartz minerals with feldspar, cementing materials, and rock fragments and contribute to sandstone's high capacity to hold crude oil in petroleum reservoirs (Waldschmidt, 1941; Bjørlykke and Jahren, 2010). The extraction of reservoir rock samples is typically achieved through specialized drilling and coring procedures conducted in petroleum reservoirs during oil and gas exploration activities (Zou et al., 2010). The coring procedure facilitates the careful extraction of reservoir rock samples, enabling comprehensive laboratory analysis and evaluation (Pellizzari et al., 2013). Following the extraction procedure, common preparations such as mechanical grinding, washing, and drying are applied to enhance the applicability of reservoir rock samples (Baraka-Lokmane et al., 2009). Owing to its mineralogical framework and porosity, sandstone obtained from oil reservoirs has broad applications, including water treatment by capturing hydrocarbons, heavy metals, and organic pollutants (Zhao et al., 2024).

Several factors affect sandstone composition, porosity, and permeability in oil reservoirs, such as grain characteristics, mineral content, fluid interfaces, and depositional environment, e.g., fluvial, marine, or aeolian (Siddiqui et al., 2017; Morad et al., 2010; Peretomode et al., 2022; Wang et al., 2019; Wilson et al., 1977; Yang et al., 2014). Diagenetic processes such as compaction, cementation, and dissolution, along with tectonic activities, including burial and fracturing, impact the quality of sandstone (Bjørlykke, 2014; Morad et al., 2010; Lander et al., 2022). These factors contribute to the coloration of sandstone, ranging from green to black, due to the presence of various chemical compounds (Hajpál et al., 2004). The predominant constituents in sandstone mostly include quartz (SiO_2), feldspar ($KAlSi_3O_8$, $NaAlSi_3O_8$, $CaAl_2Si_2O_8$), and carbonates, along with aluminum oxide (Al_2O_3) and iron oxide (Fe_2O_3), in addition to insignificant amounts of heavy minerals (Iskandarova et al., 2026). As a fundamental natural source for quartz (silicon dioxide), sandstone offers a more accessible source compared to crystalline hard rocks. High-purity quartz has become an essential mineral due to its extraordinary applications in nanotechnologies, including glass fabrication, optics, microelectronics, semiconductors, and telecommunications (Pan et al., 2022). Moreover, quartz is a primary silicon source, applied in diverse fields such as medicine, sensors, biosensing technologies, photonics, microelectronics, energy applications, and solar silicon production (Xu et al., 2021; Jennings et al., 2024). MacDonald et al. (2010) investigated sandstone in the Permian Unayzah A reservoir in Saudi Arabia, revealing the composition of quartz grains with minor feldspars, fewer lithic fragments, and minimal primary clay (MacDonald et al., 2010). Another example from Qasim Formation, Northwest Saudi Arabia, the sandstone consists of quartz, primarily monocrystalline, 20% to 67% of the composition, detrital plagioclase (trace to 1.3%), K-feldspar (trace to 0.7%), muscovite (trace to 1.5%), minor biotite (<1%), sedimentary lithic fragments and other minerals such as glauconite and zircon are present in trace amounts (≤1%) (Bello et al., 2023). The Devonian Jauf Formation consists of compact, low-porosity sandstones and shales, with some friable sandstones, composed of quartz arenites with trace amounts of feldspar and chlorite (Al-Ramadan et al., 2013). In addition, the sandstone from Burqan Formation, in Midyan Basin, northwestern Saudi Arabia, consists dominantly of quartz (80%), with feldspar (9.7%), rock fragments (10.3%), and authigenic minerals including biotite, calcite, and iron oxides (Saner et al., 2006).

In this paper, a comprehensive understanding of the physicochemical properties of reservoir-derived rock samples and their mineral components could assist in understanding this natural resource for efficient utilization, including water purification and environmental applications.

This study intends to determine the mineral composition and crystallographic properties of the investigated samples. The samples were characterized using X-ray diffraction (XRD), Fourier-transform infrared (FTIR) spectroscopy, scanning electron microscopy (SEM), energy-dispersive X-ray spectroscopy (EDS), thermogravimetric analysis (TGA), Brunauer–Emmett–Teller (BET) surface area analysis, and UV–Vis spectroscopy to evaluate their mineralogical, structural, thermal, and adsorption-related properties.

2. Geological Settings

The subsurface rock samples investigated in this study were collected during oil well drilling operations from the same well in an oil reservoir located in the Eastern Province of Saudi Arabia. The samples were obtained from two vertically separated intervals at approximately 2000 ft and 4000 ft depth. One sample was selected from each depth interval for detailed characterization. During drilling operations, lithological variations were observed between these two intervals. The 2000-ft sample revealed a black lithology, whereas a light-gray material was encountered at the greater depth (4000 ft). This visual distinction suggested potential compositional differences and motivated further investigation. The reason for selecting these two depth intervals is their direct association with differences in mineralogical composition and pore structure, consistent with the objectives of this study. However, detailed formation data were not available; therefore, the study focuses on mineralogical and depth comparisons rather than formal stratigraphic classification.

3. Materials and Methods

3.1 Acquisition of samples/Sample collection

Two reservoir rock samples were collected from an oil field reservoir located in the eastern region of Saudi Arabia, extracted from two different depths: sample 1 at 2000 ft and sample 2 at 4000 ft (Fig. 1). The reservoir rock samples exhibited different colors. Sample 1 from 2000 ft is black, while sample 2 from 4000 ft is gray. The grains in both samples exhibit variable morphology, including rounded, sub-rounded, elongated, and irregular shapes, as confirmed by SEM analysis. Equal weights of the samples were used in all experiments to maintain consistency.

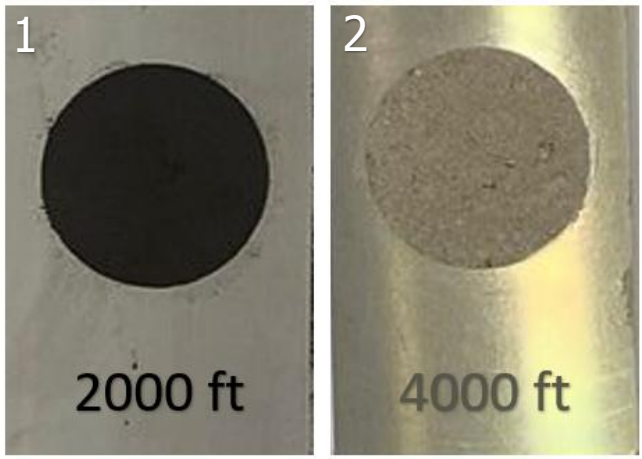

Fig. 1. Photographs of compacted powder pellets prepared from reservoir rock samples for FTIR analysis. The black pellet (left) corresponds to sample 1 collected from 2000 ft, while the light-gray pellet (right) corresponds to sample 2 collected from 4000 ft.

3.2 Sample Preparation

Each sample was ground using a natural agate mortar and pestle, and 200 mg of the powdered material was placed into separate test tubes. To each tube, 10 mL of distilled water was added. The mixtures were stirred and then heated to approximately 90°C for 10 minutes, just below the boiling point. Following heating, the samples were filtered using filter paper, and the filtrates were collected for further analysis. After 48 hours, the dried reservoir rock residues were retrieved and subjected to a series of characterization techniques to determine their mineral composition, structural features, and adsorbed organic content.

The solid-state properties of the samples were examined using Powder X-ray Diffraction (XRD), Thermogravimetric Analysis (TGA), Fourier Transform Infrared Spectroscopy (FTIR), Scanning Electron Microscopy (SEM), Energy-dispersive spectroscopy (EDS), and Brunauer-Emmett-Teller (BET) surface area analysis. Powder XRD patterns were recorded for three

replicates of each sample using a Shimadzu 6100AS diffractometer, scanning from 10° to 80° (2θ) at a rate of 2° min-1. FTIR spectra were acquired in the 4000-400 cm-1 range using a Shimadzu IR-Affinity 1S spectrophotometer and KBr pellet technique. TGA was performed using a Shimadzu TGA-50 system, heating approximately 10.674 mg of each sample in alumina crucibles at a rate of 10°C min-1 under a nitrogen atmosphere, within a temperature range of 25–700°C. Morphological analysis was carried out using a FEI Inspect S50 SEM. Elemental composition was determined through EDS analysis on a JEOL JSM-6380LA system. EDS measurements were performed as localized semi-quantitative spot analyses on selected regions of the sample surfaces to evaluate elemental composition. BET surface area and pore size distribution were measured using a Quantachrome Nova 4200e analyzer.

To evaluate the adsorption of organic pollutants, the filtrates obtained after heating and filtering the reservoir rocks-water mixtures were analyzed using Ultraviolet-Visible (UV-Vis) spectroscopy. Spectra were recorded with a Jenway 6850 UV-Vis spectrophotometer over the 200-1100 nm range, at a scan speed of 400 nm min-1.

4. Results and Discussion

4.1 X-Ray Diffraction (XRD) Pattern

Mineral phases in the samples were identified using XRD patterns, which provide valuable information about mineralogical composition through diffraction peaks corresponding to multiple crystallographic planes (Ali et al., 2022). The XRD patterns of the samples collected from 2000 ft and 4000 ft depths reveal markedly different mineralogical compositions (Fig. 2).

The X-ray diffraction (XRD) pattern of the 2000 ft sample exhibits several diffraction peaks. The reflections occur at 2θ values of 20.74°, 26.58°, 37.08°, 38.75°, 42.34°, 50.66°, 58.98°, and 67.40°, corresponding to the (100), (011), (110), (012), (111), (200), (021), and (112) crystallographic planes, respectively.

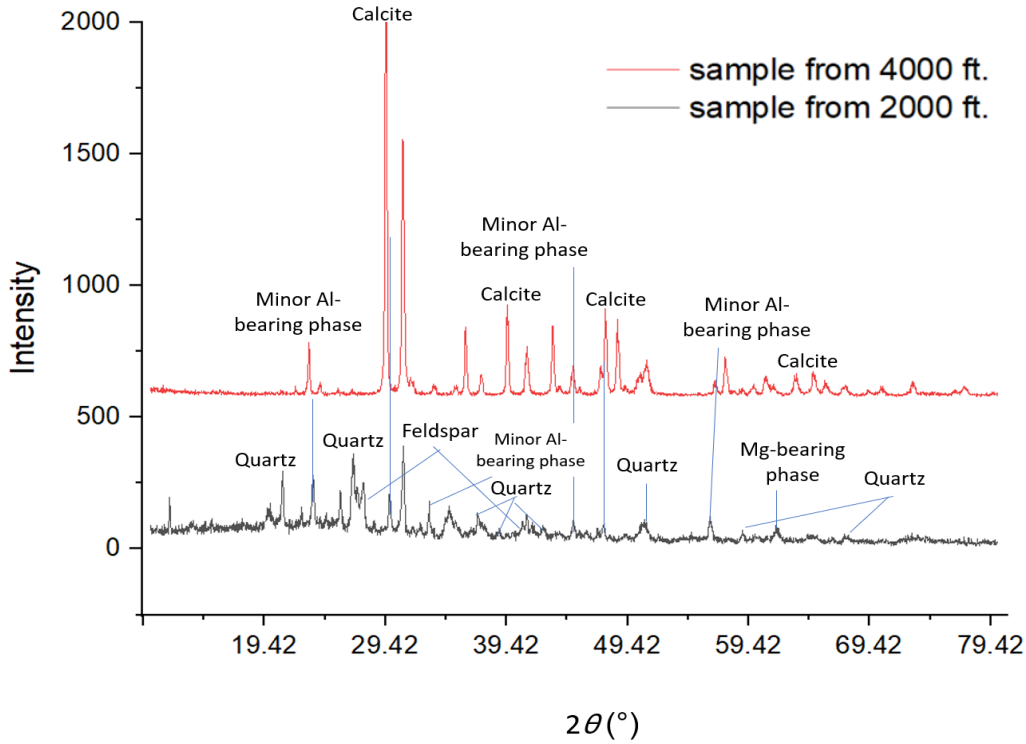

Fig. 2. XRD patterns of the reservoir-derived rock samples collected from 2000 ft and 4000 ft depths. The identified phases include quartz, feldspar, calcite, Mg-bearing phases, and minor Al-bearing phases.

These principal reflections match the standard diffraction pattern of α-quartz (JCPDS No. 45-0946), confirming its presence as the dominant mineral in the 2000 ft sample. The strong reflection near 26.58° further supports the dominance of quartz within the siliciclastic matrix. In addition to quartz, several weaker reflections corresponding to secondary mineral phases are present. Diffraction peaks at 27.46°, 30.94°, and 41.14° are attributed to feldspar minerals, specifically orthoclase (JCPDS No. 31-0966).

Minor reflections associated with calcite ($CaCO_3$) occur at ~ 29.68° and 47.48° (JCPDS No. 47-1743), suggesting limited carbonate components within the reservoir rock matrix. Additional weak peaks observed correspond to minor Mg- and Al-bearing phases commonly present as minerals in natural reservoir rocks. The detected peak positions, corresponding interplanar spacings (d-values), crystallographic planes, and JCPDS references are summarized in Table 1.

On the other hand, the XRD pattern of the 4000 ft sample is dominated by calcite reflections, demonstrating a carbonate-dominated lithology at deeper levels. The foremost diffraction peaks occur at 2θ values of 29.70°, 39.70°, 47.48°, 48.8°, and 64.9°, corresponding to the (104), (113), (018), (116), and (0012) crystallographic planes, respectively. These peaks are in very good agreement with the standard calcite diffraction pattern (JCPDS No. 47-1743), confirming calcite as the predominant mineral phase in the 4000 ft sample. The crystal system of calcite is rhombohedral, belonging to the R3c space group (167). Minor peaks detected at 43.45° and 57.76° correspond closely to Al-bearing phases (JCPDS No. 46-1212), in addition to several weak reflections attributed to minerals in natural reservoir rocks. The peak assignments and crystallographic parameters for the 4000 ft sample are presented in Table 2.

The interplanar spacing values (dhkl) were calculated using Bragg's law, $n\lambda=2d\sin\theta$, where θ is the diffraction angle, λ represents the X-ray wavelength (1.54 Å for Cu Kα radiation), and n is the diffraction order. The calculated d-spacing values for the 2000 ft sample (4.26, 3.34, 2.46, 2.24, 2.14, 2.07, 1.99, and 1.82 Å) closely correspond to the standard values of α-quartz, confirming its crystalline nature. In contrast, the calculated d-spacing values for the 4000 ft sample (3.86, 2.89, 2.29, 2.22, and 1.44 Å) are consistent with calcite and agree well with the reference pattern reported in JCPDS No. 47-1743. The XRD results clearly show a mineralogical contrast between the two depth intervals within the same well, suggesting a significant variation in mineralogical composition. The 2000-ft sample is mainly quartz-rich with minor additional phases, whereas the 4000-ft sample exhibits a carbonate-dominated composition, as evidenced by strong calcite reflections. This depth-related mineralogical contrast is emphasized in the present study; however, detailed sedimentological investigation was beyond the scope of this work.

4.2. Fourier-Transform Infrared (FTIR) Spectrum

The FTIR spectrum of the reservoir rock sample 1 from 2000 ft exhibits several peaks, indicating the presence of clay minerals, quartz, carbonates, and organic compounds (Fig. 3).

The FTIR spectra of the 2000-ft sample exhibit differences in functional group presence, indicating potential variations in diagenetic processes and mineralogical composition at different depths (Fig. 3a). The broad absorption bands around 3700 cm^{-1} and 3400 cm^{-1} correspond to O-H stretching vibrations, typically due to clay and water content in the sample. The peak at 2900 cm^{-1} suggests C-H stretching vibrations, probably related to the trace amount of organic matter. Peaks at 900 cm^{-1} and 1600 cm^{-1} correspond to Al–OH bending vibration, characteristic of clay minerals likely with aluminosilicate contribution. The Si-O stretching vibrations around 1100 cm^{-1} confirm the dominance of quartz and silicates, which are the primary

framework minerals in reservoir rocks. Lastly, the peak at 700 cm^{-1} is a key fingerprint region for quartz (Si-O-Si bending). The FTIR results imply that the reservoir rocks 2000-ft sample consists of a diverse mineralogical composition, including SiO_2 (quartz), minor Al-bearing phases, and organic traces. On the other hand, the FTIR spectrum of the 4000-ft sample shows less variety of distinctive bands than the 2000-ft sample, mostly of carbonate minerals (Fig. 3b), as also evidenced by the XRD patterns. The observed bands at ~1400–1470 cm^{-1} (CO_3 stretching) and at ~875 and ~712 cm^{-1} (CO_3 bending modes) are consistent with calcite ($CaCO_3$). An additional broad band near 3400 cm^{-1} corresponds mainly to O–H stretching vibrations associated with adsorbed water or traces of clay minerals. Compared with sample 1, the silicate bands (Si–O) are significantly reduced due to the higher carbonate content. Table 3 shows the differences between the observed peaks of both samples.

Table 1: Peak positions and JCPDS references for 2000 ft sample.

Mineral Phase	**Major observed peaks 2θ (°)**	**The dhkl interplanar spacing values (Å)**	**The crystallographic planes**	**JCPDS Reference**
Quartz	20.74, 26.58, 37.08, 38.75, 42.34, 50.66, 58.98, 67.40	4.26, 3.34, 2.46, 2.24, 2.14, 2.07, 1.99, 1.82	(100), (011), (110), (012), (111), (200), (021), (112)	JCPDS No. 45-0946
Mg- bearing phase	61.9	1.5	(220)	JCPDS No. 45-0946
$CaCO_3$	29.68, 47.48	3.86, 2.89	(104), (116)	JCPDS No. 47-1743
Feldspar (Orthoclase)	27.46, 30.94, 41.14	3.25, 2.98, 2.51	(002), (201), (132)	JCPDS No. 31-0966
Minor Al-bearing phase	34.7, 44.98, 56.10	2.55, 2.09, 1.62	(104), (113), (024)	JCPDS No. 46-1212
Others	47.46, 33.04, 33.32, 25.66, 22.42, 19.62, 11.64	2.43, 2.71, 2.69, 3.47, 3.96, 4.52, 7.61	(200), (311), (220), (400), (420), (440), (620)	

Table 2: Peak positions and JCPDS references for 4000 ft sample.

Mineral Phase	**Major observed peaks 2θ (°)**	**The dhkl interplanar spacing values (Å)**	**The crystallographic planes**	**JCPDS Reference**
$CaCO_3$	29.70, 39.70, 47.48, 48.8, 64.9	3.86, 2.89, 2.29, 2.22, 1.44	(104), (113), (018), (116), (0012)	JCPDS No. 47-1743
Minor Al-bearing phase	43.45, 57.76	2.09, 1.62	(113), (024)	JCPDS No. 46-1212
Others	23.12, 31.12, 36.18, 37.22, 41.32	4.28, 2.87, 2.48, 2.42, 2.19	(201), (132), (220), (311), (400)	

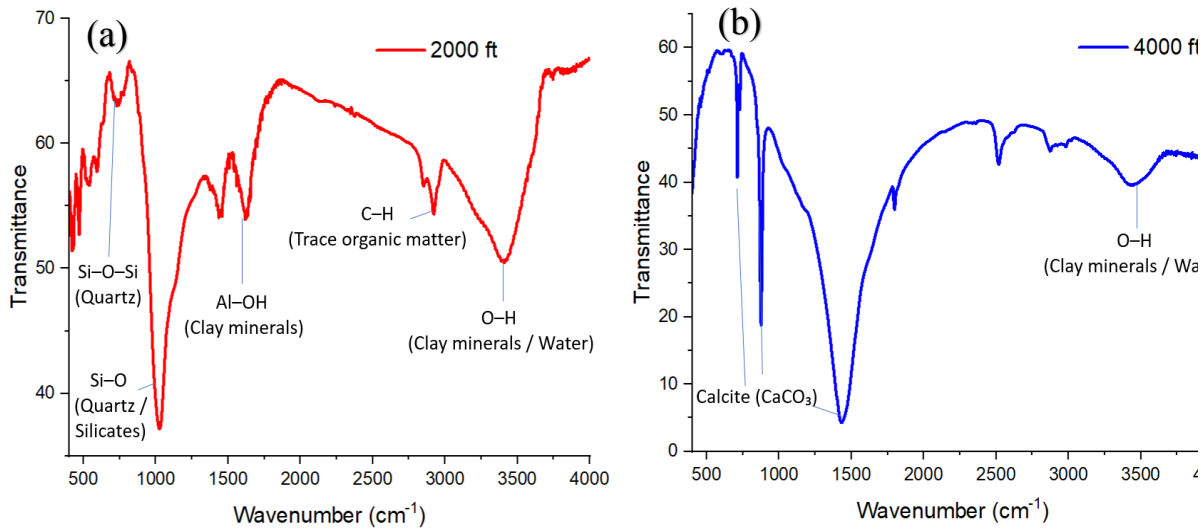

Fig. 3. FTIR spectra of the samples collected from (a) 2000 ft and (b) 4000 ft depths. The major absorption bands of the 2000 ft sample are associated with quartz/silicate minerals, clay-related components, and hydroxyl-bearing phases. In contrast, the 4000 ft sample is characterized by carbonate-related bands consistent with calcite. Mineral assignments were made based on the characteristic FTIR absorption bands of the identified phases.

Table 3: Observed peaks of FTIR analysis for 2000 ft and 4000 ft samples.

Observed Peakes	**2000 ft**	**4000 ft**
O-H Stretching (3700 and 3400 cm-1)	Present (Clay minerals, Water)	Present (Clay minerals, Water)
C-H Stretching (2900 cm-1)	Present (Trace Organic Matter)	Absent (Minor Organic Material)
Si-O Stretching (~1100 cm-1)	Present (Quartz, Silicates)	Absent
Al-OH Bending (900 and 1600 cm-1)	Present (Kaolinite, Clay Minerals)	Absent
Si-O-Si Bending (~700 cm-1)	Present (Quartz)	Absent
Additional Peaks	Si-O Stretching (~1026 cm-1), Si-O-Si Bending (~740 cm-1), Al-OH (1456 - 1635 cm-1), Carbonates, Pyrite, MgO	Dominantly Calcite (CaCO3), no Silicate Framework
Porosity and Permeability	Higher (Quartz framework intact, partial carbonate cementation)	Lower (complete silicate replacement by carbonates, reduced reservoir quality)

4.3. Scanning Electron Microscopy (SEM) Analysis

The SEM images reveal clear changes in grain morphology between the 2000-ft (Figs. 4a–d) and 4000-ft samples (Figs. 4e–g), confirming a mineralogical and microstructural variation with depth. The 2000-ft sample (Fig. 4a–b) exhibits a granular texture with visible intergranular pore spaces between sub-angular to rounded grains. A loosely packed grain framework with visible interparticle voids is observed (Figs. 4c–d). Surface irregularities and pore features are observed on some grains, possibly related to diagenetic changes (You et al., 2021). Fine-grained materials adhere to some grain surfaces, possibly indicating clay

coatings (Kang et al., 2024). In addition, fractured grain edges are present, suggesting mechanical compaction effects. The 2000-ft sample displays better preservation of intergranular spaces compared to the deeper sample. Conversely, SEM images of the 4000-ft sample (Figs. 4e–g) display a denser crystalline texture characterized by partially to well-rounded grains. The intergranular pore spaces are reduced, suggesting possible carbonate cementation compared to the shallower sample. Some fractured grains are observed; however, these fractures appear narrow and discontinuous. The grain size ranges from approximately 3 to 12 µm, with most grains clustered between 5 and 10 µm.

SEM analysis was conducted to evaluate grain morphology and surface textural characteristics at different depths. The 2000-ft sample shows clear intergranular spaces (Figs. 4a–b), whereas the 4000-ft sample exhibits a denser crystalline framework (Figs. 4e–g). Differences in grain distribution and surface texture may reflect burial modification processes (Charlaftis et al., 2022). Because the SEM micrographs were acquired at different magnifications and fields of view, comparisons of intergranular spaces are limited to qualitative observations rather than direct quantitative assessments of porosity. These observations are therefore interpreted in conjunction with BET surface area analysis for quantitative evaluation (Section 4.6).

4.4. EDS Analysis and Mineralogical Composition

The elemental composition of reservoir rock samples from 2000 ft was determined using Energy Dispersive Spectroscopy (EDS) (Table 4 and Fig. 4.h). The elemental composition was averaged from three EDS measurements to estimate the elemental distribution within the 2000-ft reservoir rock samples. The major elements detected include silicon, oxygen, carbon, aluminum, potassium, sulfur, calcium, magnesium, iron, and chlorine. Quartz (SiO_2) is inferred to be the dominant mineral phase in the reservoir rocks. The quartz content was estimated by applying the Si-to-SiO_2 conversion factor (2.14) to the average silicon content (17.12 wt%), yielding an approximate SiO_2 content of 36.64%. Notably, the oxygen content compared to silicon is consistent with the dominance of silicate minerals. The high proportion of quartz highlights the potential of the material for silica-related industrial applications such as glass and ceramic manufacturing (Shaffer, 2006).

On the other hand, the low calcium content (~2.01 wt%) indicates only minor carbonate presence. By applying the Ca-to-$CaCO_3$ conversion factor (2.50), the estimated $CaCO_3$ content is approximately 5.02%, suggesting a minor amount of calcite within the sample. The possible occurrence of Ca-bearing silicate phases may also be inferred from the combined presence of calcium and silicon within the EDS spectra. The average aluminum content (5.78 wt%) corresponds to an Al_2O_3-equivalent of approximately 10.92 wt% when expressed as oxide equivalent. This observation is consistent with the presence of Al-bearing aluminosilicate phases identified by XRD analysis.

In addition, based on the occurrence of a combination of aluminum and potassium (5.99 wt%), feldspar is expected to be present within the reservoir rock matrix. Feldspars are widely used in glass and ceramic industries and function as fluxing agents in various industrial processes (Zhang et al., 2018).

Furthermore, the presence of magnesium is approximately 1.02 wt%, corresponding to about 1.69 wt% MgO when expressed as oxide equivalent. The presence of iron is approximately 1.38 wt%.

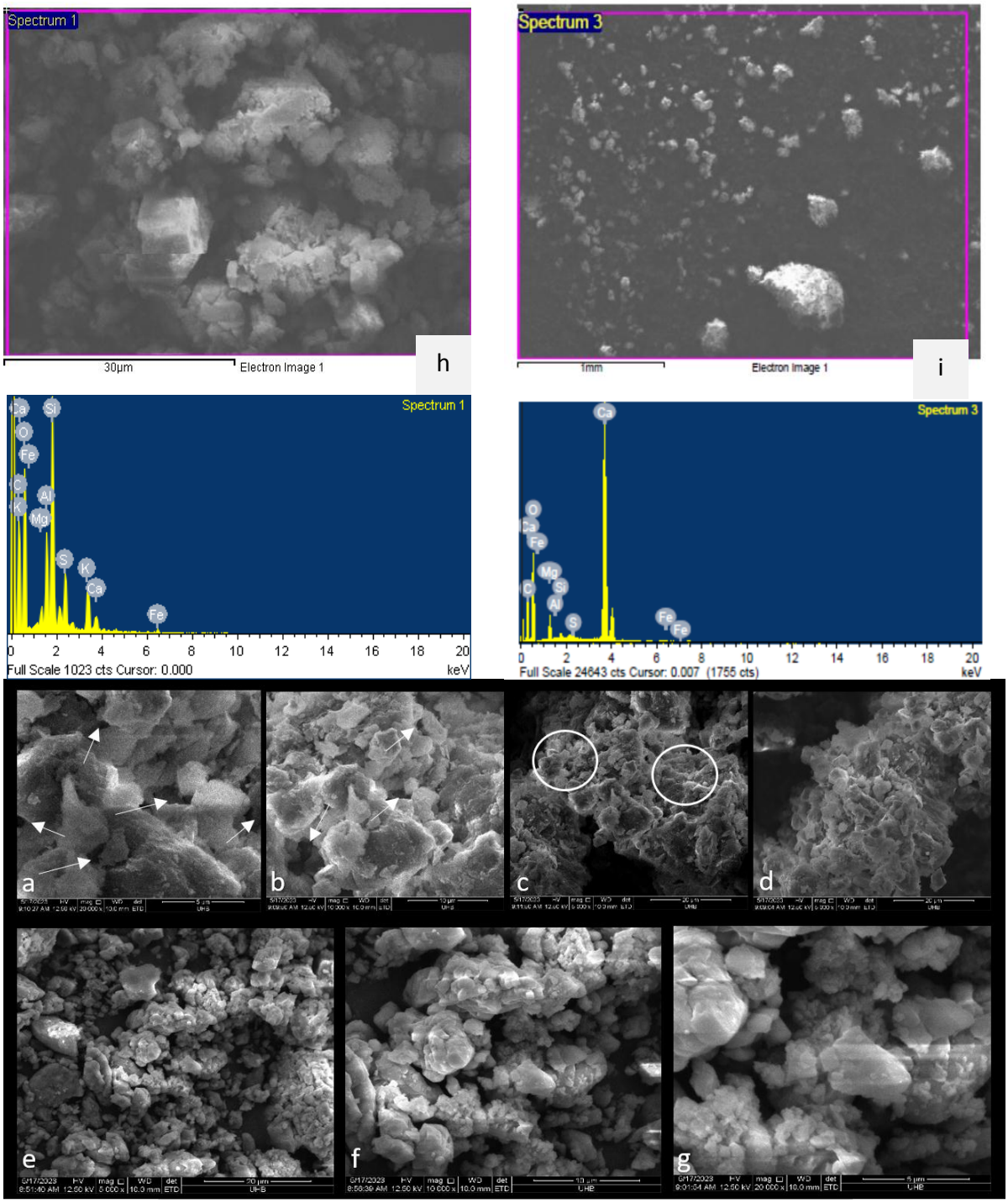

Fig. 4. Comparative SEM micrographs of subsurface reservoir samples collected from 2000 ft and 4000 ft depths. (a–d) 2000 ft sample showing intergranular pore spaces (arrows) and clay-related surface features (circles). (e–g) 4000 ft carbonate-dominated sample displaying dense crystalline texture with reduced preservation of intergranular framework; (h) EDS spectrum of the 2000 ft sample and (i) EDS spectrum of the 4000 ft sample represent the highlighted regions in the SEM micrographs and indicate the locations selected for localized semi-quantitative EDS spot analysis.

When converted using the Fe-to-FeS_2 conversion factor (2.15), the possible presence of iron sulfide minerals such as pyrite is estimated at approximately 2.97%, suggesting minor amounts of pyrite or other iron-bearing sulfide components. Interestingly, a high carbon signal (22.02 wt%) is detected in the 2000-ft reservoir rock sample. This carbon enrichment is expected to be associated with hydrocarbon adsorption from the surrounding oil reservoir

environment. Over geological time, interactions between reservoir rocks and hydrocarbon fluids may lead to the retention of organic materials within the reservoir rock framework. The porous nature of reservoir rocks, as suggested in SEM, particularly if pore spaces are present between quartz and feldspar grains, enhances the tendency of the rock to trap small organic molecules (Yang et al., 2025).

In addition, clay minerals and carbonaceous materials can act as adsorption sites. The carbon content exceeding that expected solely from carbonate minerals suggests that hydrocarbons may be retained within the pore spaces of the reservoir rocks. The adsorption of organic pollutants and heavy metals in reservoir rock systems is governed by several physicochemical interactions, including hydrogen bonding, ionic exchange, and covalent interactions. Hydrophobic interactions may also contribute to the adsorption of organic compounds within reservoir rock matrices. Moreover, porosity plays an important role in contaminant retention, allowing minerals such as feldspar to participate in the adsorption of heavy metal ions (e.g., Pb^{2+} , Cd^{2+} , and As^{3+}) through cation exchange capacity (CEC). Clay minerals such as kaolinite [$Al_2\ Si_2\ O_5\ (OH)_4$], montmorillonite [$(Na,\ Ca)_{0\ .3\ 3}\ (Al,\ Mg)_2\ (Si_4\ O_{1\ 0}\ )(OH)_2\ \cdot nH_2\ O$], and illite [$(Al_2\ )(Si_4\ -x)O_{1\ 0}\ (OH)_2\ \cdot K_1\ -x$] can further enhance adsorption capacity due to their surface area and surface charge properties (Basu et al., 2021; Surendar et al., 2025).

Additionally, pH conditions significantly influence adsorption processes. Under acidic conditions (low pH), reservoir rock surfaces may become positively charged, favoring the adsorption of anionic pollutants such as sulfates ($SO_4^{\ 2-}$) and nitrates ($NO_3^{\ -}$) (Choudhary et al., 2022). Conversely, under alkaline conditions (high pH), the surface becomes negatively charged, promoting the adsorption of cationic contaminants including heavy metal ions. Consequently, reservoir rock materials may play an important role in the removal of various contaminants, including petroleum hydrocarbons, organic solvents, pesticides, and dyes (Jo et al., 2023). Recently, combining reservoir rocks with other adsorbents such as biochar, zeolites, and activated carbon has led to the development of advanced hybrid adsorbent materials (Eniola et al., 2023). In addition to sample 1, EDS analysis was also performed on sample 2 collected from 4000 ft depth (Table 4 and Fig. 4i). The results confirm XRD and FTIR results by exhibiting a dominant presence of calcium (28.23 wt%), oxygen (52.69 wt%), and carbon (15.97 wt%), with only trace amounts of silicon (0.37 wt%) and aluminum (0.15 wt%). Additionally, the presence of minor magnesium (2.35 wt%) possibly indicates Mg-bearing carbonate phases, such as dolomite. The 2000 ft values represent the average of three localized semi-quantitative EDS spot analyses, whereas the 4000 ft values correspond to a localized semi-quantitative EDS analysis.

4.5. Brunauer–Emmett–Teller (BET) Surface Area Analysis

The BET surface area of the 2000-ft sample was measured at 23.225 m^2/g, providing quantitative insight into the surface features. This value falls within the anticipated range for natural reservoirs containing siliciclastic materials (Zhang et al., 2024; Thomas et al., 2024). This surface area is in a moderate level between high surface areas, such as zeolite ~ 100 m^2/g (Allanas et al., 2021), and low surface areas, such as calcite ~ 14 m^2/g (Schultz et al., 2013).

The moderate BET surface area of the 2000 ft sample may be attributed to the presence of intergranular pore spaces, grain surface irregularities, and minor clay-related components, rather than clay minerals alone (Charlaftis et al., 2022; Xie et al., 2022).

On the contrary, the 4000-ft sample exhibits a significantly lower BET surface area of 1.343 m^2/g. This value is consistent with its calcite-rich composition and denser crystalline framework identified in SEM micrographs (Figs. 6a–c), reducing the surface area.

In comparison, synthetic adsorbents commonly exhibit high surface areas >100 m^2/g; the BET measurement of these samples is obviously lower yet consistent with the BET measurement of natural geological materials (Zhang et al., 2024; Thomas et al., 2024). Although the adsorption capacity of these natural materials is relatively moderate to low, a surface engineering approach could potentially enhance their performance for environmental applications (Manoj et al., 2024).

The dominance of silicate minerals in the 2000-ft sample can enhance fluid adsorption due to increased surface area and interconnected pores. Additionally, the presence of clay minerals is known for their high cation exchange capacity and ability to retain fluids. The open pore network of the 2000-ft sample suggests that it remains an effective medium for hydrocarbon adsorption and reactive fluid interactions, making it a potential candidate among natural resources for adsorption applications, such as water remediation from organic pollutants.

Table 4: Elemental composition of the studied samples obtained from localized semi-quantitative EDS spot analyses.

Element (Kα)	2000 ft Weight (%)	2000 ft Atomic (%)	4000 ft Weight (%)	Weight (%) ± Uncertainty	4000 ft Atomic (%)
O	41.00	45.83	52.69	0.27	60.44
C	22.02	32.41	15.97	0.22	42.41
Si	17.12	10.90	0.37	0.03	0.24
K	5.99	2.74	–	–	–
Al	5.78	3.84	0.15	0.02	0.10
S	3.93	2.17	0.08	0.02	0.05
Ca	2.01	0.90	28.23	0.17	12.93
Fe	1.38	0.44	0.15	0.04	0.05
Mg	1.02	0.75	2.35	0.05	1.78
Cl	0.55	0.28	–	–	–
Total	**~100**	–	**100**	–	**100**

4.6. Thermogravimetric Analysis (TGA)

Thermogravimetric analysis (TGA) was conducted on reservoir rock samples from 2000 and 4000 ft depths to assess mineral decomposition, volatile content, and thermal stability. Figure 7(a-b) shows the thermal behaviors of both samples separately, suggesting differences in mineral decomposition among the two depths.

The 2000-ft sample exhibits a high total mass loss (~46.16%), indicating the loss of a significant proportion of volatile components. The initial mass loss below 200 °C (~4.5%) is mainly attributed to the release of adsorbed and bound water (Fig. 5a). The major mass loss between 300–600 °C suggests the presence of organic materials and/or structural hydroxyl groups associated with clay minerals (Fig. 5d). These components are expected to decompose or undergo dehydroxylation within this temperature range, resulting in the observed weight loss.

In contrast, the 4000-ft sample shows a lower total weight loss (~14.17%), consistent with a mineralogically more stable composition (Fig. 5b). The initial mass loss below 200 °C (~7.03%) is likely related to moisture release. The second weight-loss stage observed between 500–600 °C (~7.14%) is attributed to the thermal decomposition of calcite ($CaCO_3 \rightarrow CaO + CO_2$). This observation is consistent with the predominance of carbonate phases identified by XRD analysis. The substantially lower overall mass loss of the 4000-ft sample supports its carbonate-dominated and thermally stable nature compared to the shallower 2000-ft sample.

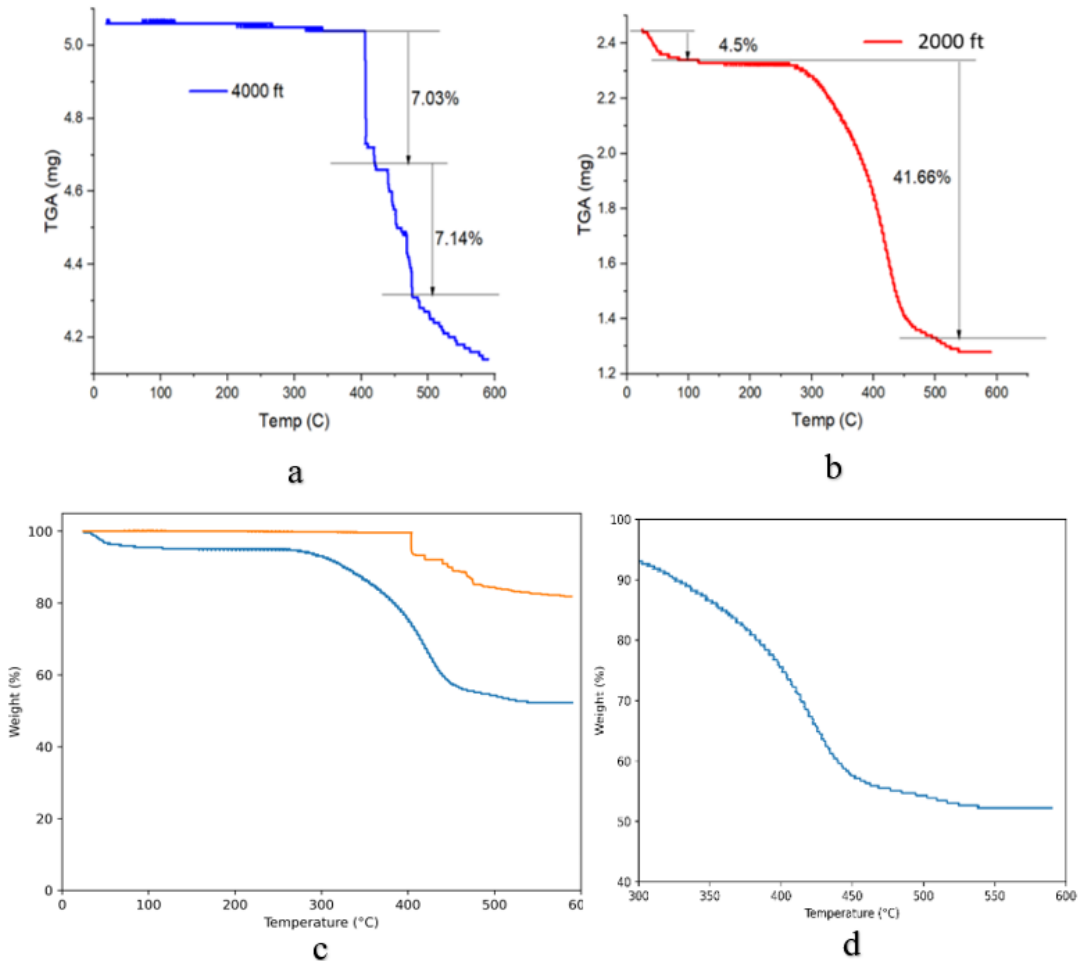

Fig. 5. (a) TGA analysis curves for the 2000-ft sample. (b) TGA analysis curves for the 4000-ft sample. (c) Normalized TGA curves of the 2000 ft (below) and 4000 ft (above) samples plotted on the same scale for comparison. (d) Enlarged view of the major mass-loss region (300–600 °C) of the 2000 ft sample, highlighting the dominant thermal decomposition stage.

For accurate comparison, all TGA curves were normalized to the initial mass (100%) (Fig. 5c). This thermal behavior further reflects the mineralogical differences between the two samples and their potential influence on adsorption performance.

4.7. UV-Vis Analysis of Water Samples Filtered from Stirred and Heated Reservoir Rock Solutions

The UV-Vis absorbance spectra of water samples filtered from stirred and heated reservoir rocks solutions at 2000 ft and 4000 ft depths reveal interpretation in dissolved organic components within the reservoir rocks matrix (Fig. 6). The absorbance (λmax) for the 2000 ft sample occurs at 214 nm, while for the 4000 ft sample, it is at 268 nm (Fig. 6). These distinctions offer contrasts in dissolved species, assumed to be affected by the mineral composition.

The 2000 ft sample exhibits a strong UV absorbance peak at 214 nm, typically associated with π→π* electronic transitions found in simple conjugated organic compounds, such as alkenes, or unsaturated compounds (Prasad et al., 2025). Since the 2000-ft reservoir rocks sample originates from an oil reservoir, the UV-Vis peak at 214 nm is expected to correspond to dissolved oil residues, including conjugated organic compounds. The higher intensity indicates a more significant presence of dissolved organic compounds, which may have been released due to mechanical stirring and heating during the experiment (Ahmad et al., 2023). This supports the idea that the 2000 ft reservoir rocks retain organic residues due to their moderate porosity, releasing organic matter into the water. Similar results were

observed where higher UV absorbance at shorter wavelengths was linked to reservoir rocks with greater hydrocarbon saturation (Si et al., 2021; Abbas et al., 2022).

The 4000 ft sample, on the other hand, shows an absorbance peak at 268 nm, characteristic of n→π* electronic transitions correlated with heavier aromatics (Proos Vedin et al., 2024). Porosity at this depth might be diminished, but small pores can still trap hydrocarbons. The lower absorbance intensity compared to the 2000 ft sample suggests a smaller amount of dissolved organic compounds is present, due to deeply buried and compacted reservoir rocks, leading to diminished adsorption potential. The contrast in UV absorption peaks between the two depths highlights the impact of mineralogical alterations on adsorption efficiency.

5. Comparison with Similar Studies and Future Perspectives

The current study offers a comprehensive characterization of a black reservoir rock sample obtained from an oil reservoir in eastern Saudi Arabia, highlighting its mineral composition, pore structure, and adsorption potential. Compared to similar studies on natural adsorbents such as activated carbon, zeolites, and other reservoir rock samples from various geological formations, the findings of this research reveal notable distinctions. While synthetic adsorbents like activated carbon exhibit significantly higher BET surface areas (typically between 500–1500 m^2/g), they are also associated with higher production costs and environmental impacts (Foo and Hameed, 2010; Mohan and Pittman, 2007; Ioannidou and Zabaniotou, 2007). In contrast, the 2000-ft black reservoir rocks sample analyzed in this study presents a moderate BET surface area of 23.225 m^2/g, indicating a favorable capacity for adsorbing organic compounds and hydrocarbons. These values align with or exceed those reported in natural reservoir rocks from formations such as the Qasim, Burqan, and Jauf, where quartz-dominated mineralogy and minor feldspar and clay contents are common (Zaid, 2013).

Furthermore, compared to reservoir rocks studied in the Unayzah A reservoir, the black reservoir rocks here show an enhanced ability to retain and release hydrocarbons, confirmed by UV–Vis analysis, which detected organic residues released after thermal treatment (Zhang et al., 2018).The presence of clay-related components and feldspar in the 2000-ft sample further improves its adsorption potential, as these components offer additional adsorption sites and influence the surface charge properties of the rock under varying pH conditions (Sparks, 2003; Stumm et al., 1996; Sposito, 2008).

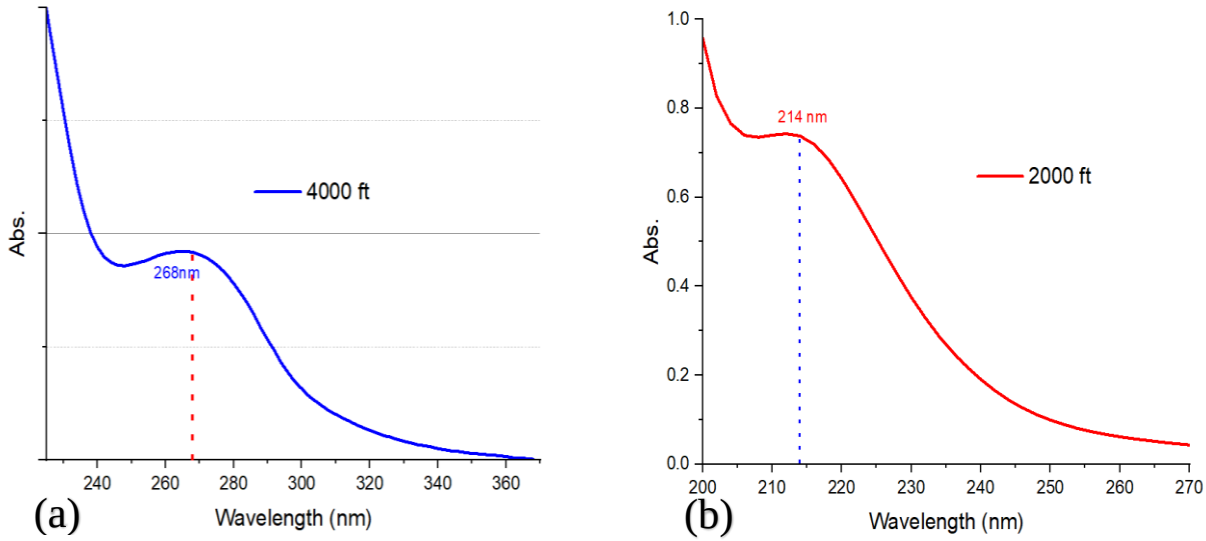

Fig. 6. UV-Visible absorption spectra of reservoir rock samples collected from 2000 ft (a) and 4000 ft (b) depths.

Unlike other studies that mainly describe reservoir rocks' geological or compositional attributes, this work integrates experimental techniques, including XRD, FTIR, SEM, TGA, EDS, BET, and UV–Vis spectroscopy, to evaluate the adsorptive behavior and structural evolution under burial conditions. Notably, the study suggests depth-related mineralogical variation at 4000 ft, characterized by increased carbonate dominance, which may influence porosity and permeability (Morad et al., 2010; Paxton et al., 2002). This comparative analysis reinforces the relevance of geological depth, mineral diagenesis, and pore evolution in determining reservoir rocks' environmental and industrial utility (Morad et al., 2010; Worden and Morad, 2003).

Looking ahead, this work opens promising avenues for future research and practical applications. One potential direction involves enhancing the adsorption performance of reservoir rocks through surface modification techniques, such as acid treatment, nanoparticle functionalization, or integration with bio-based materials to create composite adsorbents (Wang and Peng, 2010). These approaches may significantly increase surface area, adsorption site density, and selectivity toward specific pollutants (Khezami and Capart, 2005). Additionally, given the black reservoir rock's strong light absorption and high carbon content, there is potential to explore its application in energy-related technologies. Investigating its optical properties through bandgap measurements and photocurrent response analysis could determine its suitability for photovoltaic devices, solar water purification systems, or photocatalytic reactors (Kumar et al., 2018). Its use in optoelectronics and environmental photodetectors is another exciting possibility. On a larger scale, pilot studies can be designed to test reservoir rocks-based filtration columns for treating oil-contaminated water or industrial effluents, particularly in arid regions where reservoir rocks are abundant and economically feasible. Integrating geochemical simulations and adsorption isotherm modeling can also provide deeper insights into the molecular-level interactions between pollutants and reservoir rock surfaces (Bansal et al., 2005; Gupta and Suhas, 2009). Detailed petrographic investigation was beyond the scope of the present study; however, future petrographic analysis would provide additional constraints on lithological classification and diagenetic interpretation.

This study not only advances our understanding of the mineralogical and adsorption properties of reservoir rocks but also underscores their significant potential in environmental remediation and emerging energy applications. With appropriate surface modifications and further exploration, black reservoir rocks could become a sustainable and cost-effective alternative to synthetic adsorbents, offering practical benefits in water treatment, hydrocarbon recovery, and renewable energy sectors.

6. Conclusion

This study presents a comparative characterization of subsurface reservoir-derived rock samples collected from 2000 ft and 4000 ft within the same well in eastern Saudi Arabia, focusing on depth-related mineralogical and adsorption-related variations.

First, mineralogical analysis (XRD and FTIR) reveals a clear compositional difference with depth: the 2000-ft sample is dominated by silicate minerals (quartz, feldspar, and clay-related phases), whereas the 4000-ft sample shows carbonate dominance with calcite as the primary phase.

Second, SEM observations indicate differences in grain arrangement and pore structure, where the shallower sample displays a relatively more open granular framework compared to the denser carbonate-rich structure observed at 4000 ft.

Third, TGA, UV–Vis, and BET analyses highlight functional differences between the two intervals. The 2000-ft sample exhibits higher volatile-related mass loss, detectable hydrocarbon-related absorption features, and a moderate specific surface area (23.225 m^2/g), whereas the deeper carbonate-dominated sample shows

significantly lower surface area and reduced adsorption-related characteristics.

The results demonstrate that mineralogical variation with burial depth within the same well influences the structural and adsorption-related properties of reservoir-derived materials, providing a basis for further evaluation of their potential in adsorption-related environmental applications.

Acknowledgments

The author would like to acknowledge the University of Hafr Al Batin for the support and facilities. The author also acknowledges the Research Laboratory at King Saud University for providing access to the equipment used in this study. Special thanks are extended to Kawthar Mustafa for her assistance in obtaining the rock samples used in this research.

Data Availability Statement

The data that support the findings of this study are available from the corresponding author upon reasonable request.

References

Abbas, A. H., Moslemizadeh, A., Sulaiman, W. R. W., Jaafar, M. Z., & Pourafshary, P. (2022). Lignin adsorption in sandpacks during horizontal flow using UV–Vis spectrometry as a quantification tool. *Arabian Journal of Geosciences*, *15*(6), 501. DOI: 10.1007/s12517-022-09770-4

Ahmad, A., Ali, M., Al-Sehemi, A. G., Al-Ghamdi, A. A., Park, J.-W., Algarni, H., & Anwer, H. (2023). Carbon-integrated semiconductor photocatalysts for removal of volatile organic compounds in indoor environments. *Chemical Engineering Journal*, *452*, 139436. DOI: 10.1016/j.cej.2022.139436.

Ali, A., Chiang, Y. W., & Santos, R. M. (2022). X-ray diffraction techniques for mineral characterization: A review for engineers of the fundamentals, applications, and research directions. *Minerals*, *12*(2), 205. https://doi.org/10.3390/min12020205

Allanas, E., Rahman, A., Arlin, E., & Prasetyanto, E. A. (2021). Study surface area and pore size distribution on synthetic zeolite X using BET, BJH and DFT methods. In Journal of Physics: Conference Series (Vol. 2019, No. 1, p. 012094\). IOP Publishing. https://doi.org/10.1088/1742-6596/2019/1/012094

Al-Ramadan, K., Morad, S., Norton, A. K., & Hulver, M. (2013). Linking diagenesis and porosity preservation versus destruction to sequence stratigraphy of gas condensate reservoir sandstones; the Jauf Formation (Lower to Middle Devonian), Eastern Saudi Arabia. In S. Morad, J. M. Ketzer, & L. F. De Ros (Eds.), *Linking Diagenesis to Sequence Stratigraphy* (pp. 297–335). Wiley-Blackwell. https://doi.org/10.1002/9781118485347.ch13

Arsalan, N., Palayangoda, S. S., Burnett, D. J., Buiting, J. J., & Nguyen, Q. P. (2013). Surface energy characterization of sandstone rocks. *Journal of Physics and Chemistry of Solids*, *74*(8), 1069–1077. https://doi.org/10.1016/j.jpcs.2013.02.027

Bansal, R. C., & Goyal, M. (2005). *Activated carbon adsorption*. CRC Press. https://doi.org/10.1201/9781420028812

Baraka-Lokmane, S., Main, I. G., Ngwenya, B. T., & Elphick, S. C. (2009). Application of complementary methods for more robust characterization of sandstone cores. *Marine and Petroleum Geology*, *26*(1), 39–56. https://doi.org/10.1016/j.marpetgeo.2007.11.003

Basu, A., & Mookherjee, M. (2021). Intercalation of water in kaolinite ($Al_2Si_2O_5(OH)_4$) at subduction zone conditions: Insights from Raman spectroscopy. *ACS Earth and Space Chemistry*, *5*(4), 834–848. https://doi.org/10.1021/acsearthspacechem.0c00349

Bell, F. G. (1992). The durability of sandstone as building stone, especially in urban environments. *Bulletin of the Association of Engineering Geologists*, *24*, 49–60.

Bello, A. M., Al-Ramadan, K., Koeshidayatullah, A. I., Amao, A. O., Herlambang, A., Al-Ghamdi, F., & Malik, M. H. (2023). Impact of magmatic intrusion on diagenesis of shallow

marine sandstones: An example from Qasim Formation, Northwest Saudi Arabia. *Frontiers in Earth Science, 11*, 1105547. https://doi.org/10.3389/feart.2023.1105547

Bjørlykke, K. (2014). Relationships between depositional environments, burial history and rock properties: Some principal aspects of diagenetic process in sedimentary basins. *Sedimentary Geology, 301*, 1–14. https://doi.org/10.1016/j.sedgeo.2013.12.002

Bjørlykke, K., & Jahren, J. (2010). Sandstones and sandstone reservoirs. In K. Bjørlykke, *Petroleum geoscience: From sedimentary environments to rock physics* (pp. 113–140). Springer. https://doi.org/10.1007/978-3-642-02332-3

Cao, Y., Wang, Y., Zhang, Z., & Wang, H. (2022). Recycled sand from sandstone waste: A new source of high-quality fine aggregate. *Resources, Conservation and Recycling, 179*, 106116. https://doi.org/10.1016/j.resconrec.2022.106116

Chakraborty, R., Asthana, A., Singh, A. K., Jain, B., & Susan, A. B. H. (2022). Adsorption of heavy metal ions by various low-cost adsorbents: A review. *International Journal of Environmental Analytical Chemistry, 102*(2), 342–379. https://doi.org/10.1080/03067319.2020.1722811

Charlaftis, D., Dobson, K. J., Jones, S. J., Lakshtanov, D., Crouch, J., & Cook, J. (2022). Experimental simulation of burial diagenesis and subsequent 2D-3D characterization of sandstone reservoir quality. *Frontiers in Earth Science, 10*, 766145. https://doi.org/10.3389/feart.2022.766145

Choudhary, M., Muduli, M., & Ray, S. (2022). A comprehensive review on nitrate pollution and its remediation: Conventional and recent approaches. *Sustainable Water Resources Management, 8*(4), 113. https://doi.org/10.1007/s40899-022-00631-1

Eniola, J. O., Sizirici, B., Fseha, Y., Shaheen, J. F., & Aboulella, A. M. (2023). Application of conventional and emerging low-cost adsorbents as sustainable materials for removal of contaminants from water. *Environmental Science and Pollution Research, 30*(38), 88245–88271. https://doi.org/10.1007/s11356-023-28399-8

Foo, K. Y., & Hameed, B. H. (2010). Insights into the modeling of adsorption isotherm systems. *Chemical Engineering Journal, 156*(1), 2–10. https://doi.org/10.1016/j.cej.2009.09.013

Gupta, V. K., & Suhas. (2009). Application of low-cost adsorbents for dye removal—A review. *Journal of Environmental Management, 90*(8), 2313–2342. https://doi.org/10.1016/j.jenvman.2008.11.017

Hajpál, M., & Török, Á. (2004). Mineralogical and colour changes of quartz sandstones by heat. *Environmental Geology, 46*(3), 311–322. https://doi.org/10.1007/s00254-004-1034-z

Ioannidou, O., & Zabaniotou, A. (2007). Agricultural residues as precursors for activated carbon production—A review. *Renewable and Sustainable Energy Reviews, 11*(9), 1966–2005. https://doi.org/10.1016/j.rser.2006.03.013

Iskandarova, M. I., Atabaev, F. B., & Khadzhiev, A. Sh. (2026). Utilization of natural silicate rocks to reduce the carbon footprint in the cement industry. *Kompleksnoe Ispolzovanie Mineralnogo Syra = Complex Use of Mineral Resources, 338*(3), 40–50. https://doi.org/10.31643/2026/6445.27

Jennings, A., Senior, A., Guerin, K., Main, P., & Walsh, J. (2024). A review of high-purity quartz for silicon production in Australia. *Australian Journal of Earth Sciences, 71*(8), 1085–1097. https://doi.org/10.1080/08120099.2024.2362296

Jo, T., Tsuri, K., Hirohara, T., & Yamanaka, H. (2023). Warm temperature and alkaline conditions accelerate environmental RNA degradation. *Environmental DNA, 5*(5), 836–848. https://doi.org/10.1002/edn3.334

Kang, Y., Zhu, R., Liu, K., Zhang, J., & Zhang, S. (2024). Detrital and authigenic clay minerals in shales: A review on their identification and applications. *Heliyon, 10*(20), e39239. https://doi.org/10.1016/j.heliyon.2024.e39239

Khezami, L., & Capart, R. (2005). Removal of chromium(VI) from aqueous solution by activated carbons: kinetic and equilibrium studies. *Journal of Hazardous Materials*, *123*(1–3), 223–231. https://doi.org/10.1016/j.jhazmat.2005.04.012

Kumar, S., Gupta, R.C., & Shrivastava, S. (2017). Effective utilization of quartz sandstone mining wastes: A technical note on its thermal resistance. *Journal of Cleaner Production*, *140*, 1129-1135. https://doi.org/10.1016/j.jclepro.2016.10.053

Kumar, S., Thomas, B.S., Gupta, V., Basu, P., & Shrivastava, S. (2018). Sandstone wastes as aggregate and their usefulness in cement concrete – A comprehensive review. *Renewable and Sustainable Energy Reviews*, *81*, 1147-1153. https://doi.org/10.1016/j.rser.2017.08.044

Lander, R. H., Bonnell, L. M., Taylor, T. R., & Espejo, I. (2022). Reservoir quality and diagenesis of deepwater sandstones. In *Deepwater Sedimentary Systems: Science, Discovery and Applications* (pp. 471–514). Elsevier. https://doi.org/10.1016/B978-0-323-91918-0.00011-6

MacDonald, R., Hardman, D., Sprague, R., Meridji, Y., Mudjiono, W., Galford, J., Rourke, M., Dix, M., & Kelton, M. (2010). Using elemental geochemistry to improve sandstone reservoir characterization: A case study from the Unayzah A interval of Saudi Arabia. *SPWLA 51st Annual Logging Symposium*, Perth, Australia.

Manoj, G. M., Shalini, M., Thenmozhi, K., Ponnusamy, V. K., & Hari, S. (2024). Recent advancements in the surface modification and functionalization of magnetic nanomaterials. *Applied Surface Science Advances*, *21*, 100608. https://doi.org/10.1016/j.apsadv.2024.100608

Mohan, D., & Pittman, C. U. (2007). Arsenic removal from water/wastewater using adsorbents—A critical review. *Journal of Hazardous Materials*, *142*(1–2), 1–53. https://doi.org/10.1016/j.jhazmat.2006.01.006

Morad, S., Al-Ramadan, K., Ketzer, J. M., & De Ros, L. F. (2010). The impact of diagenesis on the heterogeneity of sandstone reservoirs: A review of the role of depositional facies and sequence stratigraphy. *AAPG Bulletin*, *94*(8), 1267–1309. https://doi.org/10.1306/04211009178

Noruzi, Y., Sharifi, M., Fahimpour, J., Sabet, M., Akbari, M., & Hosseini, S. (2024). The State-of-the-Art of wettability alteration in sandstones and Carbonates: A mechanistic review. *Fuel*, *356*, 129570. https://doi.org/10.1016/j.fuel.2023.129570

Pan, X., Li, S., Li, Y., Guo, P., Zhao, X., & Cai, Y. (2022). Resource, characteristic, purification and application of quartz: A review. *Minerals Engineering*, *183*, 107600. https://doi.org/10.1016/j.mineng.2022.107600

Paxton, S. T., Szabo, J. O., Ajdukiewicz, J. M., & Klimentidis, R. E. (2002). Construction of an intergranular volume compaction curve for evaluating and predicting compaction and porosity loss in rigid-grain sandstone reservoirs. *AAPG Bulletin*, *86*(12), 2047–2067. https://doi.org/10.1306/61EEDDFA-173E-11D7-8645000102C1865D

Pellizzari, L., Neumann, D., Alawi, M., Voigt, D., Norden, B., & Würdemann, H. (2013). The use of tracers to assess drill-mud penetration depth into sandstone cores during deep drilling: Method development and application. *Environmental Earth Sciences*, *70*(8), 3727–3738. https://doi.org/10.1007/s12665-013-2715-2

Peretomode, E., Oluyemi, G., & Faisal, N. H. (2022). Oilfield chemical-formation interaction and the effects on petrophysical properties: A review. *Arabian Journal of Geosciences*, *15*(13), 1223. https://doi.org/10.1007/s12517-022-10469-9

Prasad, S. G., Lal, C., Verma, K. C., & Rao, D. P. (2025). Reaction mechanism chemistry of chain scission, crosslinking, and other product formation in γ-ray irradiated PET polymer using molecular spectroscopy. *Chemistry Africa*, *8*, 2409–2420. https://doi.org/10.1007/s42250-025-01253-9

Proos Vedin, N., Escayola, S., Radenković, S., Solà, M., & Ottosson, H. (2024). The n,π* states of heteroaromatics: When are they the lowest excited states and in what way can they

be aromatic or antiaromatic? *The Journal of Physical Chemistry A, 128*(22), 4493–4506. https://doi.org/10.1021/acs.jpca.4c02580

Saner, S., Hassan, H. M., Al-Ramadan, K. A., & Abdulghani, W. M. (2006). Mineralogical, pore and petrophysical characteristics of the Devonian Jauf Sandstone reservoir, Hawiyah field, eastern Saudi Arabia. *Journal of Petroleum Geology, 29*(3), 257–272. https://doi.org/10.1111/j.1747-5457.2006.00257.x

Schultz, L. N., Andersson, M. P., Dalby, K. N., Müter, D., Okhrimenko, D. V., Fordsmand, H., & Stipp, S. L. S. (2013). High surface area calcite. *Journal of Crystal Growth, 371*, 34–38. https://doi.org/10.1016/j.jcrysgro.2013.01.049

Shaffer, N. R. (2006). The time of sands: Quartz-rich sand deposits as renewable resource. *Electronic Green Journal*, (24).

Si, Q. H., Li, J. G., Miao, P. S., Zhang, C., Zhu, Q., & Zhao, H. L. (2021). Characteristics and mechanism of hydrocarbon alteration of faded sandstone in the uranium-bearing Luohe Formation, Pengyang area, southwestern Ordos Basin. *Ore Geology Reviews, 139*, 104500. https://doi.org/10.1016/j.oregeorev.2021.104500

Siddiqui, N. A., Rahman, A. H. A., Sum, C. W., Yusoff, W. I. W., & Ismail, M. S. (2017). Shallow-marine sandstone reservoirs, depositional environments, stratigraphic characteristics and facies model: A review. *Journal of Applied Sciences, 17*, 212–237. https://doi.org/10.3923/jas.2017.212.237

Sparks, D. L. (2003). Environmental Soil Chemistry. Academic Press. ISBN: 978-0-12-656446-4

Sposito, G. (2008). The Chemistry of Soils (2nd ed.). Oxford University Press. ISBN: 978-0-19-531369-7

Stumm, W., & Morgan, J. J. (1996). *Aquatic Chemistry: Chemical Equilibria and Rates in Natural Waters* (3rd ed.). John Wiley & Sons.

Surendar, K., Rajkumar, P., Balachandran, V., & Arun, B. (2025). FT-IR, XRD, EDX-SEM and radiological fingerprints of sedimentary rocks of Bodamalai Hills in Tamil Nadu, India. *Indian Journal of Science and Technology, 18*(1), 59–71. https://doi.org/10.17485/IJST/v18i1.2783

Thomas, S., Umar, A., Yunarti, R. T., Bakri, R., Putra, B. R., Wahyuni, W. T., Arifutzzaman, A., Aroua, M. K., & Khalil, M. (2024). Mesoporous metal oxide via nanocasting: Recent advances on types of templates, properties, and catalytic activities. *Materials Today Communications, 40*, 110152. https://doi.org/10.1016/j.mtcomm.2024.110152

Waldschmidt, W. A. (1941). Cementing materials in sandstones and their probable influence on migration and accumulation of oil and gas. *AAPG Bulletin, 25*(10), 1839–1879.

Wang, J., Cao, Y., Xiao, J., Liu, K., & Song, M. (2019). Factors controlling reservoir properties and hydrocarbon accumulation of the Eocene lacustrine beach-bar sandstones in the Dongying Depression, Bohai Bay Basin, China. *Marine and Petroleum Geology, 99*, 1–16. https://doi.org/10.1016/j.marpetgeo.2018.09.022

Wang, S., & Peng, Y. (2010). Natural zeolites as effective adsorbents in water and wastewater treatment. *Chemical Engineering Journal, 156*(1), 11–24. https://doi.org/10.1016/j.cej.2009.10.029

Wilson, M. D., & Pittman, E. D. (1977). Authigenic clays in sandstones: Recognition and influence on reservoir properties and paleoenvironmental analysis. *Journal of Sedimentary Petrology, 47*(1), 3–31.

Worden, R. H., & Morad, S. (2003). Clay minerals in sandstones: Controls on formation, distribution and evolution. In R. H. Worden & S. Morad (Eds.), *Clay Mineral Cements in Sandstones* (International Association of Sedimentologists Special Publication 34, pp. 3–41). Blackwell Publishing.

Worden, R. H., Armitage, P. J., Butcher, A. R., Churchill, J. M., Csoma, A. E., Hollis, C., Lander, R. H., & Omma, J. E. (2018). Petroleum reservoir quality prediction: Overview and

contrasting approaches from sandstone and carbonate communities. *Geological Society, London, Special Publications, 435*, 1–31. https://doi.org/10.1144/SP435.21

Xie, W., Chen, S., Vandeginste, V., Yu, Z., Wang, H., & Wang, M. (2022). Review of the effect of diagenetic evolution of shale reservoir on the pore structure and adsorption capacity of clay minerals. *Energy & Fuels, 36*(9), 4728–4745. https://doi.org/10.1021/acs.energyfuels.2c00675

Xu, H., Zhou, W., Hu, Q., Yi, T., Ke, J., Zhao, A., Lei, Z., & Yu, Y. (2021). Quartz types, silica sources and their implications for porosity evolution and rock mechanics in the Paleozoic Longmaxi Formation shale, Sichuan Basin. *Marine and Petroleum Geology, 128*, 105036. https://doi.org/10.1016/j.marpetgeo.2021.105036

Yang, C., & Yang, E. (2025). Mineral composition and pore structure on spontaneous imbibition in tight sandstone reservoirs. *Scientific Reports, 15*(1), 7504. https://doi.org/10.1038/s41598-025-89676-9

Yang, R., Fan, A., van Loon, A. J., Han, Z., & Wang, X. (2014). Depositional and diagenetic controls on sandstone reservoirs with low porosity and low permeability in the eastern Sulige gas field, China. *Acta Geologica Sinica – English Edition, 88*(5), 1513–1534. https://doi.org/10.1111/1755-6724.12315

You, J., & Lee, K. J. (2021). Pore-scale study to analyze the impacts of porous media heterogeneity on mineral dissolution and acid transport using Darcy–Brinkmann–Stokes method. *Transport in Porous Media, 137*(3), 575–602. https://doi.org/10.1007/s11242-021-01577-3

Zaid, S. M. (2013). Provenance, diagenesis, tectonic setting and reservoir quality of the sandstones of the Kareem Formation, Gulf of Suez, Egypt. *Journal of African Earth Sciences, 85*, 31–52. https://doi.org/10.1016/j.jafrearsci.2013.04.010

Zhang, B., Ren, G., Ran, L., Liu, M., Geng, P., & Yi, W. (2024). Green synthesis of biomass-derived porous carbon for electrochemical detection of heavy metal ions: Methods, properties, and applications. *Journal of Environmental Chemical Engineering, 12*(5), 113903. https://doi.org/10.1016/j.jece.2024.113903

Zhang, Y., Hu, Y., Sun, N., Liu, R., Wang, Z., Wang, L., & Sun, W. (2018). Systematic review of feldspar beneficiation and its comprehensive application. *Minerals Engineering, 128*, 141–152. https://doi.org/10.1016/j.mineng.2018.08.043

Zhao, Y., Chang, C., Ji, H., & Li, Z. (2024). Challenges of petroleum wastewater treatment and development trends of advanced treatment technologies: A review. *Journal of Environmental Chemical Engineering, 12*(5), 113767. https://doi.org/10.1016/j.jece.2024.113767

Zou, C., Zhang, G., Tao, S., Hu, S., Li, X., Li, J., Dong, D., Zhu, R., Yuan, X., Hou, L., Qu, H., Zhao, X., Jia, J., Gao, X., Guo, Q., Wang, L., & Li, X. (2010). Geological features, major discoveries and unconventional petroleum geology in global petroleum exploration. *Petroleum Exploration and Development, 37*(2), 129–145. https://doi.org/10.1016/S1876-3804(10)60021-3